JOURNAL OF THERMOPHYSICS AND HEAT TRANSFER
Vol. 23, No. 2, April–June 2009

Global Temperature-Sensitive Paint System for Heat Transfer Measurements in Long-Duration Hypersonic Flows

Inna Kurits* and Mark J. Lewis†
University of Maryland, College Park, Maryland 20742

DOI: 10.2514/1.39926

A quantitative global intensity-based temperature-sensitive paint heat transfer measurement system has been developed at Arnold Engineering Development Center Hypervelocity Wind Tunnel No. 9. The system has been designed for use with metal wind-tunnel models in long-duration (on the order of seconds) hypersonic flows. A numerical finite differencing scheme has been proposed for calculating convective heat flux from the paint's surface emission intensity data. As part of the development effort, surface emission intensity data have been collected on a model of a NASA Orion Crew Exploration Vehicle capsule in Mach 10 flow. The proposed data reduction algorithm has been applied to generate high-resolution quantitative heat transfer maps of the model's heat shield. Good quantitative agreement has been achieved between the heat transfer maps and the baseline conventional instrumentation data on the majority of the heat shield surface.

Nomenclature

d	=	insulative layer thickness
I	=	intensity
i	=	time index
j	=	space index
K	=	thermal conductivity
L	=	temperature-sensitive coating thickness
M_∞	=	freestream Mach number
Po	=	total pressure
$\dot{q}$	=	heat transfer rate per unit area
R	=	heat shield radius
R^2	=	square of the correlation coefficient of a linear fit
Re	=	unit Reynolds number
r	=	radial distance from the center of the heat shield
ref	=	reference (wind off) quantity
St	=	Stanton number
s	=	surface quantity
T	=	temperature
t	=	time
x	=	distance normal to model's surface; roll axis of the model
y	=	pitch axis of the model
z	=	yaw axis of the model
α	=	thermal diffusivity
Δt	=	time step size
Δx	=	differential element size
∇T	=	temperature gradient

I. Introduction

PEAK surface heat flux is a critical design parameter for most vehicles that are expected to experience high aerodynamic heating loads for at least a portion of their trajectories. This includes the majority of hypersonic vehicles. For instance, heat transfer rates are extremely important in design of a thermal protection system for an atmospheric reentry vehicle, such as the NASA Orion Crew Exploration Vehicle (CEV).

Commonly, time-resolved quantitative heat transfer measurements in hypersonic ground test facilities involve discrete instrumentation, such as thermocouples, Schmidt–Boelter gauges, thin-film gauges, and others [1,2]. Although these methods are well established, they can only provide measurements at discrete locations where the sensors are installed. This makes important flow phenomena such as boundary-layer transition, flow separation, and shock–boundary-layer interactions hard to detect. These types of phenomena typically exhibit strong spatial heating gradients. It is difficult to resolve them using discrete measurements unless the instrumentation density is very high or there is an indication before the test of where the phenomena of interest may occur. There are other reasons for seeking alternatives. For instance, installation of large arrays of discrete instrumentation is not cost effective and can be labor intensive. Some model areas, such as sharp leading edges or thin walls, may be hard or impossible to instrument with discrete sensors. Discrete instrumentation can be intrusive, so great care must be taken to not alter a surface geometry of a test article during the installation process.

Global heat transfer measurement systems, on the other hand, are typically less intrusive than discrete sensors. They can provide high-resolution qualitative and quantitative heat transfer maps of an entire model surface, which is their most attractive advantage over discrete instrumentation. Additionally, they can be applied to almost any model shape, usually at a lower cost per application. Some examples of global heat transfer measurement techniques are temperature-sensitive paints (TSP), thermographic phosphors, liquid crystals, and infrared thermography.

An effort to develop a global quantitative heat transfer measurement system was undertaken at the Arnold Engineering Development Center (AEDC) Hypervelocity Wind Tunnel No. 9 (Tunnel 9). Tunnel 9 is a hypersonic blowdown wind tunnel with long run times (on the order of seconds) as compared to other hypersonic facilities with similar freestream conditions (i.e., high Mach and Reynolds numbers). Initial development efforts concentrated on demonstrating the survivability of the paint system in the harsh environment of the facility. The resulting intensity-based TSP system was tested on a wedge with a protruding fin model in Mach 10 and 14 flows. High-resolution temperature maps of complex, 3-D surfaces were acquired during the test, and the paint's survivability was successfully demonstrated. However, no quantitative heat transfer data were acquired during this test. The system and experimental results from its use have been reported in

Presented as Paper 3947 at the 26th AIAA Aerodynamic Measurement Technology and Ground Testing Conference, Seattle, WA, 23–26 June 2008; received 25 July 2008; revision received 17 November 2008; accepted for publication 1 December 2008.

*Graduate Research Assistant, Department of Aerospace Engineering; currently Project Engineer, Aerospace Testing Alliance, Arnold Engineering Development Center, White Oak, Silver Spring, Maryland 20903. Student Member AIAA.

†Professor, Department of Aerospace Engineering. Fellow AIAA.

[3]. Continued system development efforts resulted in a TSP system capable of high-resolution qualitative, as well as quantitative, global heat transfer measurements. The system was tested on a model of NASA's Orion CEV capsule in Mach 10 flow in 2006. Detailed description of the test, the data processing, initial data reduction techniques, and some preliminary results are reported in [4]. The results reported in [4], however, do not include any quantitative global heat transfer maps.

Present work builds on the analysis presented in [4] and describes a modified heat transfer data reduction algorithm. Global quantitative heat transfer maps of the model's heat shield, obtained using this modified approach, are presented. Good agreement between the TSP heat transfer data and the conventional instrumentation data (i.e., thermocouples), collected during a non-TSP run at the same freestream conditions, is demonstrated.

II. Temperature-Sensitive Paint Background

Temperature-sensitive paints have been in use since the 1980s and are based on luminescence quenching mechanisms. These coatings are typically composed of a host material, usually a polymer, and luminescent molecules, dispersed within the host material, or binder. In general, the binder and the luminophores are dissolved in a solvent, which allows the coating to be applied to a model's surface with a brush or a spray [5].

The luminophores in these coatings become excited when illuminated with a light of an appropriate wavelength (usually UV or blue). The resulting fluorescence is red-shifted relative to the excitation wavelength. Fluorescence is a radiative deexcitation process, that is, it is accompanied by photon emission. Fluorescence is less likely to occur with increasing temperature because the excited molecules are more likely to take thermal paths to deexcitation (i.e., become thermally quenched). The inverse relationship between the temperature and the radiant intensity of these molecules can be established via a calibration process and allows using TSP as a temperature sensor [5]. The surface temperature data obtained during a wind-tunnel test can be used to calculate the surface convective heating rates, which are usually of primary interest in hypersonic flows. An in-depth discussion of luminescent processes is provided in [6]. More information on luminescent paints and paint systems can be found in [5,7].

III. Data Reduction Techniques for Global Heat Transfer Measurement Systems in Hypersonic Facilities

A number of global heat transfer measurement techniques have been used at various hypersonic ground test facilities over the years (e.g., TSP, thermographic phosphors, liquid crystals, infrared thermography). In most cases, temperature data are acquired first and are subsequently used to calculate the convective heat transfer on the surface. Typically, the surface convective heat transfer is not calculated directly, but is rather inferred from the heat conducted into the model at the surface boundary. In all cases, reducing global temperature data into heat flux is a difficult task. Simplifying assumptions related to specific test conditions usually have to be made to develop a practical data reduction methodology. These simplifying assumptions depend on the facility where the system is used and the types of models tested at the facility. Several examples of the heat transfer data reduction methodologies applied to coating-based global measurement systems at various hypersonic wind tunnels are summarized next.

A two-color thermographic phosphor technique has been successfully applied to ceramic wind-tunnel models at NASA Langley Research Center [8,9]. The phosphor-coated test articles at a uniform initial temperature are injected into the flow when the desired test conditions have been established in the test cell. This allows modeling the heating load as a constant step input in the heat-flux data reduction algorithm. Semi-infinite wall is assumed (i.e., no temperature rise on the back wall), which is valid for ceramic models of an appropriate thickness. Additionally, phosphor coating of negligible thickness, large local radius of curvature, and heat propagation normal to the model's surface (i.e., one-dimensional heat conduction) are assumed [9]. Applying this set of assumptions to the 1-D heat conduction equation yields a simple solution, which only requires an initial temperature image and a single run temperature image to calculate the surface convective heat transfer. In other words, the temperature time history is not required.

Roberts and East [10] describe a heat transfer data reduction methodology for a liquid crystal thermography technique applicable to hypersonic flows with durations on the order of 1 s. The technique involves matching of the thermal product $\sqrt{\rho c K}$ of the model material with that of the liquid crystals. This ensures a homogeneous thermal behavior of the test article so that a one-layer conduction heat transfer model can be used. Additionally, a constant step convective heating load, 1-D heat conduction, and semi-infinite model wall are assumed, just as in the previously described method. As a result, a straightforward analytical solution is possible. The step heating load assumption limits the applicability of this methodology to shock tunnels or facilities where models are injected into the flow after the steady freestream conditions have been achieved.

A TSP system has been successfully used for heat transfer measurements in the Japan Aerospace Exploration Agency Hypersonic Shock Tunnel facility by Nakakita et al. [11]. In that case, the heat transfer data reduction algorithm is simplified by applying a very thin TSP layer to the test articles. If the layer is sufficiently thin, the influence of the typically insulative coating on the model's surface temperature response is negligible. Using tabulated polymer material properties, the authors estimated that the influence of the luminescent paint layer can be neglected if its thickness is less than 1 μm, resulting in a less than 2% error in the heat transfer rate calculations. Ignoring the paint layer allows for the assumption of a uniform, semi-infinite medium in the heat transfer rate calculation, making the data reduction straightforward. Nagai et al. [12] conducted a follow-up experimental study to evaluate this data reduction approach. They tested ceramic models coated with a very thin luminescent paint layer (0.2–3 μm) and applied the 1-D, semi-infinite heat conduction model described by Nakakita et al. [11] for the heat transfer rate calculations. Nagai et al. [12] ignored the TSP layer in the algorithm and calculated the error associated with this simplification. They concluded that the paint layer can be ignored in the data reduction if its thickness is less than 0.5 μm, as opposed to 1 μm, as was previously estimated by Nakakita et al. [11]. The discrepancy is explained by the differences between the actual TSP material properties and the tabulated polymer material properties used in the initial study. Additionally, it was found that the error in calculated heat flux changed nonlinearly with the change in the paint layer thickness.

Hubner et al. [13] used TSP with metal test articles to measure global surface heat flux in short-duration hypersonic flow (run times on the order of 10 ms) at the LENS I shock tunnel at Calspan–University at Buffalo Research Center. A thick, insulating polyurethane layer ($\sim$100–150 μm) was applied between the thin ($\sim$5–10 μm) active luminescent paint layer and the metal model surface. The thick insulating layer has been used with metal test articles in short-duration hypersonic flows to prevent heat conduction into the test article's wall, thus allowing a one-layer (i.e., homogenous wall) assumption in the data reduction. The heat transfer was calculated assuming 1-D heat conduction, a constant step input heating load, semi-infinite wall, and temperature-independent thermophysical properties (i.e., K and α) of the TSP formulation. These assumptions are only applicable because of the impulsive nature of the facility.

Fluorescent paint use for heat transfer measurements on a waverider model was reported in 1995 at AEDC Hypervelocity Wind Tunnel No. 9 [14]. In the experiment, the aluminum model's windward surface was covered with an insulative white Mylar film ($\sim$0.1 mm thick), over which the temperature-sensitive coating was applied ($\sim$10 μm thick). The convective heat flux on the surface was calculated using Fourier's law of conduction discretized over the insulating layer as follows: $\dot{q}_s(t) = K[T_s(t) - T_b]/d$, where K is the thermal conductivity of the Mylar film, $T_s(t)$ is measured by the fluorescent coating, and T_b is the temperature at the interface

between the insulating layer and the metal base. The latter is assumed to be equal to the model's initial temperature. This model assumes linear temperature gradient through the insulating layer, ignores the fluorescent paint layer in the thermal modeling, and assumes the base temperature T_b is constant for the duration of a run (i.e., short run times and/or moderate heat fluxes). The knowledge of the thermal conductivity of Mylar is also required.

Taking into consideration the uncertainties in measured quantities (i.e., T_s and T_b), variations in the reported K values for Mylar ($\pm 20\%$), and the deviation of T_b from the initially measured value, the overall uncertainty in the heat transfer calculated using this methodology was estimated to be $\pm 21\%$ for an aluminum model and $\pm 25\%$ for a steel model [14]. In addition to the large uncertainty in the reported K value for Mylar, problems may be encountered in trying to apply the film to complex-shaped models. Additionally, the constant T_b assumption breaks down for long run times and/or high heating rates.

The present work is aimed at describing the development of a global TSP heat transfer measurement system that does not require an insulative layer, but instead, the heat conduction into the metal test article is dealt with through the use of an appropriate data reduction algorithm.

IV. Tunnel 9 Facility Description

Tunnel 9 is a blowdown facility that uses pure nitrogen as the working fluid and currently operates at Mach numbers of 7, 8, 10, and 14. The unit Reynolds number range for the facility is from $\sim 0.164 \times 10^6$/m (useful for high-altitude/viscous interaction simulation) to $\sim 157.5 \times 10^6$/m (duplication of flight dynamic pressure). The run times range between 0.25 and 15 s, depending on the freestream conditions. The test section is ~ 3.7 m long and has a diameter of ~ 1.5 m, enabling testing of large-scale model configurations. The test cell features a model support system that is capable of dynamically pitching large test articles through an angle-of-attack sweep from -5 to $+45$ deg at rates of up to 60 deg/s during a typical run. A more complete description of the Tunnel 9 facility and its capabilities can be found in [15].

V. Challenges Associated with Quantitative Global Heat Transfer Measurements at Tunnel 9

The choice of a global heat transfer measurement technique and a data reduction algorithm implemented at each test facility depend on the operational characteristics of the facility. Some of the primary challenges associated with developing a high-productivity TSP system for the use at a hypersonic blowdown wind tunnel such as Tunnel 9 are summarized next.

High dynamic and thermal loading environment (i.e., large freestream Reynolds numbers) necessitates the use of robust stainless steel models for force-and-moment testing. It is desired to use the same test articles for TSP measurements as for force-and-moment tests to reduce the cost and complexity of a test program to a customer wanting to collect several types of data at once. The temperature-sensitive coating must also be sufficiently robust to survive the tunnel test conditions.

Other challenges include relatively long run times, nonnegligible tunnel startup time, and ramplike startup heating profiles. The test articles typically experience a significant temperature rise (tens to hundreds of degrees Celsius depending on the local geometry and the freestream conditions) as a result of the long run times. This means the semi-infinite wall assumption is invalid most of the time even if an insulative layer is used between the TSP layer and the metal base. The startup time and the heating profile are important because the test articles are not injected into the flow and are subjected to heating during the startup portion of a run. This in turn complicates the data reduction, that is, step input heating cannot be assumed. Some of these challenges are illustrated in Fig. 1, where the startup and the "good flow" periods are marked on the plot of the total pressure versus time for a $M_\infty = 10$, $Re = 16.4 \times 10^6$/m run. The startup time and the useful flow period for this condition are approximately

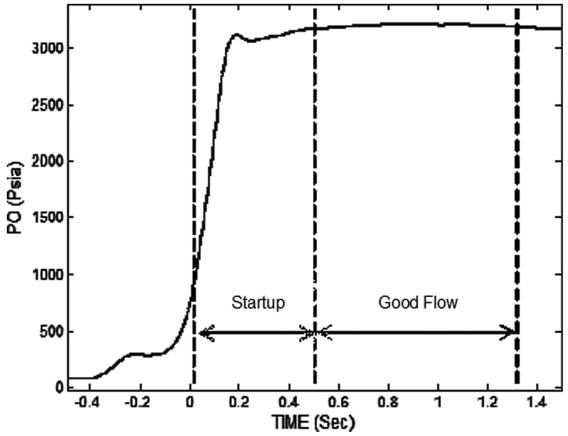

Fig. 1 Nozzle supply total pressure versus time for a static $M_\infty = 10$, $Re = 16.4 \times 10^6$/m run.

0.5 and 1 s, respectively. The run time is considered long for a hypersonic wind tunnel with such high Reynolds numbers. Finally, it is desired to have the capability to perform the global heat transfer measurements while dynamically pitching a model during a run. This has a potential to significantly increase the productivity and the cost effectiveness of the system, but at the same time imposes additional requirements on all of its components.

VI. Temperature-Sensitive Paint System Development at Tunnel 9

The TSP system presented here is capable of acquiring multiple high-resolution images during a run. It incorporates a data reduction methodology suitable for the models and test conditions typical of the facility. The methodology was developed based on the numerical scheme currently used at Tunnel 9 to calculate the convective surface heat transfer from coaxial thermocouple data. The system was tested on a model of a NASA Orion CEV capsule. The overall heat-flux data reduction approach was validated by calculating the heat flux at one location on the model and comparing it to the expected value, as described in [4]. However, no global quantitative heat transfer maps were obtained in the previous work. In the present work, the heat transfer data reduction methodology was modified, and global quantitative heat transfer maps of the model's heat shield were obtained for two of the TSP runs.

A. TSP System Specifications

Photon Technologies 200-W mercury-xenon arc lamps were chosen as the illumination source for this system. The selection was based on their stability, intensity, and operational qualities assessed in the study described in [3]. The lights are filtered with UG-1 bandpass filters centered at 355 nm to match the excitation wavelength of the TSP formulation. These filters have ~ 53 nm full width at half-maximum (FWHM). The lamps are operated continuously, that is, not flashed.

Princeton Instruments/Acton PhotonMax 512B cameras were chosen as the photodetection devices to enable acquisition of continuous, high-quality images required for quantitative time-resolved heat transfer measurements. These cameras feature a cooled 512×512 pixel charge-coupled device (CCD) array and a 16-bit A/D converter. The CCD chips in these cameras are back-illuminated and have a quantum efficiency of over 90% at the emission wavelength of the TSP formulation. The cameras are equipped with the broadband bandpass filters centered at 600 nm (with ~ 80 nm FWHM) to match the emission wavelength of the TSP formulation.

The temperature-sensitive coating was developed by LeaTech, LLC [3]. The TSP formulation uses a Europium complex as the temperature-sensitive luminophore. This paint formulation has a broad absorption spectrum (relative to Europium alone) with excitation centered at 365 nm and emission centered at 614 nm. Use

of Europium gives this formulation temperature sensitivity on the order of tenths of a degree Fahrenheit. The luminophore is combined with a high-temperature polyurethane binder resulting in a coating that can withstand temperatures up to 360°F (∼182°C) [3].

B. Heat Transfer Data Reduction Approach

Reduction of the TSP global temperature data into convective heat transfer rates requires a number of simplifying assumptions. The approach chosen at each wind tunnel depends on the facility itself. The heat transfer data reduction technique developed at Tunnel 9 was formulated to be compatible with the operational behavior of the facility. An important consideration was the need to use structurally robust stainless steel models that are well suited for force-and-moment testing in the high Reynolds number environment.

Additional factors that influenced the data reduction algorithm include the tunnel startup time, which is on the order of 500 ms (see Fig. 1). The heating profiles during part of the startup are ramplike because models are located in the flow (not injected) while the facility is started. This means that a step change in heat transfer rate cannot be assumed, as in the cases of short-duration hypersonic facilities [13] or model injection into an established flow [8]. Ultimately, it is desired to acquire the TSP data while dynamically pitching models during a single run. In this case, the heating input to a model is a function of the angle of attack, and thus it is also a function of time.

Other factors that must be accounted for in the data reduction include the highly nonlinear temperature-dependent thermophysical properties (i.e., K and α) of the paint formulation over the range of temperatures encountered in Tunnel 9 [4], that is, K and α of the coating cannot be assumed constant in the data reduction. This means that either the thermophysical properties need to be accurately measured over the appropriate temperature range, or a data reduction technique that does not require the knowledge of the thermophysical properties must be devised. An additional complication is that the temperature-sensitive coating is an insulator with a thermal conductivity several orders of magnitude lower than that of steel. The difference in the K values of the coating and the substrate requires the use of a two-layer conduction model, that is, homogenous thermal behavior of a test article coated with a TSP layer cannot be assumed.

In general, the algorithm developed to calculate the convective heat flux from the TSP data at Tunnel 9 is based on the same analysis that is applied to reducing the coaxial thermocouple temperature data into heat transfer at the facility. Following the data reduction techniques described in Sec. III, convective heat flux is found by calculating the heat conducted into the test article at the surface in the direction normal to the surface. The data reduction algorithm cannot be used in the areas where significant lateral heat conduction effects are present, unless an appropriate correction is applied. This is true for both the TSP and the coaxial thermocouple data reduction techniques.

The algorithm for coaxial thermocouple data reduction can be summarized as follows. A time history of the measured surface temperature is applied as a boundary condition in a solution of the transient, 1-D, heat conduction model. A second-order, Euler-explicit, finite difference approximation method is used to solve the transient 1-D heat conduction equation as shown in Eq. (1). The solution provides a 1-D temperature distribution at nodes at varying depths through a steel model wall of finite thickness at each time step of the algorithm. The local surface convective heat transfer rate is calculated based on the heat conducted into the model wall. More specifically, Fourier's law is solved at the surface boundary using a second-order approximation of the temperature profile at the model's surface [Eq. (2)]:

$$\frac{T_{i+1,j} - T_{i,j}}{\Delta t} = \alpha\left(\frac{T_{i,j+1} - 2T_{i,j} + T_{i,j-1}}{\Delta x^2}\right) \tag{1}$$

$$\dot{q}_{i+1,j} = \frac{-K}{2\Delta x}\left(-3T_{i+1,j} + 4T_{i+1,j+1} - T_{i+1,j+2}\right) \tag{2}$$

At the beginning of the run (initial condition), the model is assumed to be at a uniform initial temperature. Zero heat transfer at the back wall inside the model is the remaining boundary condition required to solve the heat conduction equation numerically. The latter assumption has been validated for the thick-walled models (∼0.375 in. or 0.953 cm) that are typically tested at Tunnel 9.

To develop an analogous data reduction methodology for evaluating the heat transfer using the TSP data, a second layer comprising the temperature-sensitive coating was added to the 1-D heat transfer model described previously. In reality, the temperature-sensitive coating consists of two layers: the base coat and the active layer. However, the two layers can be treated as one in the data reduction algorithm. They are made of the same host matrix material, and thus it is reasonable to assume that they have approximately the same thermophysical properties.

The two-layer numerical model is represented schematically in Fig. 2. In the figure, T_1 is the surface temperature and $T_2, T_3, \ldots, T_n$ are the temperatures inside the model wall at node locations along the axis normal to the surface. K and α with subscripts 1 and 2 are the material properties of the TSP formulation and steel, respectively. In this case, the TSP data provide the input boundary condition T_1 at the surface of the model. The heat-flux balance at the interface between the two materials (the TSP and the steel wall) is enforced using Fourier's law. One additional assumption is made to simplify the algorithm: the ∇T through the paint layer is assumed to be linear. This assumption eliminates the need to solve for the internal temperature distribution within the thin (relative to the base) TSP layer. In this case, the interface temperature T_2 can be solved for by simply discretizing Fourier's law over the interface node, as shown in Eq. (3). After finding T_2, the algorithm proceeds in exactly the same way as described previously for coaxial thermocouples:

$$K_1 \frac{T_1 - T_2}{L} = K_2 \frac{T_2 - T_3}{\Delta x} \tag{3}$$

The linear ∇T through the paint layer assumption was evaluated using a two-layer 1-D simulation created in ANSYS finite element modeling software. The finite element model was representative of a Tunnel 9 test article coated with a TSP layer. Several likely paint layer thicknesses and heating loads were tested. It was found that, in all cases examined, the error in calculated heat flux associated with the linear ∇T assumption would be on the order of 1–2% during the good flow period of a typical Tunnel 9 run. For a more detailed description of the study and the results, refer to [16].

This methodology was used in [4] to reduce the data from the NASA Orion CEV TSP test at a single point on the model's surface and validate the overall data reduction approach. In this previous work, $K_1(T)$ was estimated using the TSP and thermocouple data from the test itself because the actual thermophysical properties of the coating are uncertain. In the present work, a further simplification is made to the data reduction algorithm to eliminate the need for $K_1(T)$, as well as other parameters associated with the TSP layer, such as L and T_1. In doing so, any uncertainty in calculated heat flux associated with these parameters is also eliminated.

This simplified data reduction method requires that several thermocouples (∼6–8) are installed on the surface of the test article at locations that are representative of the range of temperatures that the model is expected to experience. Subsequently, the entire model is

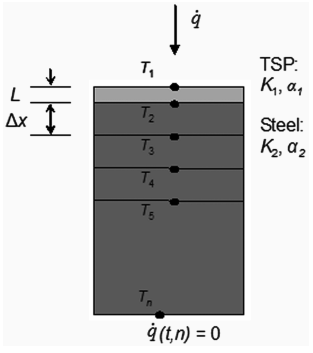

Fig. 2 Schematic of the two-layer numerical model.

coated with the TSP, including all of the thermocouples. The measured paint emission intensity can then be anchored directly to the painted thermocouple temperature readings at each thermocouple location to create an in situ calibration. The TSP measurements are thus anchored directly to the thermocouple temperature readings, which have uncertainties of 2.2°C or 0.75% of the measured value, whichever is greater [17].

The calibration, which relates the TSP emission intensity to the temperature under the paint layer, can be applied to the entire model to create a time-resolved sequence of global temperature maps. These global temperature maps can subsequently be used as boundary conditions in a one-layer heat transfer data reduction algorithm identical to the one used for coaxial thermocouple data reduction. This results in global convective heat transfer maps of a model's surface at any desired point in time (assuming 1-D heat conduction assumption holds). The justification for this simplification to the data reduction scheme is as follows.

Starting with the linear ∇T through the temperature-sensitive coating layer assumption and expressing the heat transfer balance at the interface of the two layers, as is done in Eq. (3), the terms can be rearranged to solve for the thermal conductivity of the coating as follows:

$$K_1 = K_2 \frac{L}{\Delta x} \frac{T_2 - T_3}{T_1 - T_2} \tag{4}$$

Substituting Eq. (4) into Eq. (5), which is the same as Eq. (2), but applied over the TSP layer shown in Fig. 2, and simplifying the common terms yields the expression in Eq. (6):

$$\dot{q} = \frac{-K_1}{L}\left[-3T_1 + 4\left\{\frac{1}{2}(T_1 + T_2)\right\} - T_2\right] \tag{5}$$

$$\dot{q} = \frac{K_2}{\Delta x}(T_2 - T_3) \tag{6}$$

Equation (6) is the final expression for the surface convective heat transfer when the ∇T through the TSP layer is assumed to be linear. It is also the first-order approximation of the heat flux at the interface between the TSP layer and the metal base. The absence of any terms related to the TSP layer in Eq. (6) implies that, whenever the ∇T through the paint layer is linear, the surface heat transfer can be calculated directly from the painted thermocouple data as if there were no paint layer. In other words, the coating can be ignored in the thermal model once a liner ∇T through the TSP layer has been established. The advantage of this approach is that no knowledge of the properties of the paint, the coating thickness, or even of the temperature on the surface of the test article is required to calculate the convective surface heat flux. Another advantage is that the already existing one-layer thermocouple data reduction code can be used for the heat transfer calculations.

C. NASA Orion Crew Exploration Vehicle Temperature-Sensitive Paint Test

A TSP test program was conducted on a model of the NASA Orion CEV capsule as a part of the TSP system development effort. Before the TSP test, extensive aerothermodynamic testing of the model was conducted at Tunnel 9. The 7-in.-diam (17.78-cm-diam) stainless steel model was instrumented with 100 coaxial gauges to measure surface temperature and heat transfer and to provide an indication of the boundary-layer-transition location. Following the completion of that test program, the temperature-sensitive coating was applied to the test article, and a five-run TSP test program was conducted. The main objectives of the program were to implement the system improvements that resulted from the feasibility and trade studies described in [3] and evaluate the system's ability to obtain high-resolution qualitative, as well as quantitative, global heat-flux measurements.

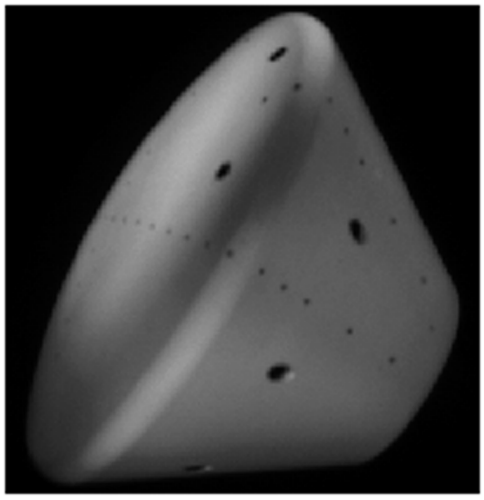

Fig. 3 Orion CEV capsule model coated with TSP and illuminated with UV light.

During the Tunnel 9 TSP tests, the pitch angle was fixed at 28 deg for all five runs. The test article coated with the TSP and illuminated with a UV light source is shown in Fig. 3. Note that only the heat shield data from runs 3 and 5 are presented and analyzed in this work. The test matrix containing the run conditions and the camera settings for the heat shield camera for the two runs is shown in Table 1. A more detailed description of the experimental setup can be found in [4].

The paint was applied to both the heat shield and the aft body of the test article over the majority of the coaxial thermocouples that were included in it to measure the heat transfer at discrete locations during the non-TSP runs of the test program. A few thermocouples were left unpainted on the heat shield for comparison with symmetrically located painted thermocouples. The unpainted areas on the model appear as large black circles in Fig. 3. The small black dots on the surface of the paint are the registration marks necessary for mapping the 2-D TSP camera images onto a 3-D grid of the test article.

The test article was repainted after the fourth run due to some physical damage to the coating that occurred as a result of small particles impacting the model and leaving small dents on the surface of the paint. The damage resulted from the combination of severe test conditions (i.e., $Re = 32.8 \times 10^6/\text{m}$) and the blunt model shape. For less severe test conditions and/or less blunt body shape (e.g., wedge in Mach 10 and 14 flows, as described in [3]), no significant damage to the coating was observed.

For each of the two paint applications, the coating thickness was measured using a magnetic induction pencil-type probe designed for measurements on metal substrates. One hundred measurements were made at discrete locations on the heat shield and the aft body to assess the uniformity of the coating. These measurements were used to calculate the average thickness of the coating for each paint application. The average paint layer thicknesses were found to be 2.1 mil (~53 μm) with a standard deviation of 0.15 mil (~3.81 μm) and 1.7 mil (~43 μm) with a standard deviation of 0.16 mil

Table 1 Run conditions and camera settings

Run	Paint application no.	M_∞	Unit Re, 10^6/m	Nominal good flow, s	CCD array binning (heat shield camera)	Frame rate, fps	Spatial resolution, cm/pixel	Exposure time, ms
3	1	10	16.4	0.4–1.3	2 × 2	~42	~0.069	~1.9
5	2	10	16.4	0.4–1.3	2 × 2	~42	~0.069	~1.9

($\sim$4.06 μm) for the first and second paint applications, respectively. These thicknesses are larger than those used by most facilities employing TSP for global heat transfer measurements. In the case of Tunnel 9, the thick coating is desired to increase the paint's emission so that good signal-to-noise ratios can be obtained, even for short exposure times. Short exposure times are necessary to freeze the motion of a vibrating model during a run.

VII. Results and Discussion

A. Calibration

For this calibration procedure, a sequence of good flow images from each of the runs was examined, and six painted-over thermocouples were selected from each run. The main thermocouple selection criteria for the calibration procedure were as follows: 1) the selected thermocouples cover the range of temperatures that the test article experienced during a run, and 2) there were no localized time-varying heating spikes/variations due to particle impacts at the locations of the selected thermocouples. The second criterion is necessary because the TSP coating tends to create a lag in the thermocouple readings due to its insulative nature, which means that some of the rapid temperature changes may not be transmitted appropriately to the thermocouples. This in turn may result in a bad calibration.

Once the thermocouples were identified for the calibration procedure, their temperature readings were matched to the surface TSP ratioed intensity values at corresponding locations and times. The resulting calibration curves with corresponding equations and squares of correlation coefficients for runs 3 and 5 are shown in Figs. 4 and 5, respectively. Note that, although the two calibrations are slightly different, as would be expected because the paint applications for the two runs were different, they are both linear. These calibrations were applied to the TSP data to convert the ratioed intensity values into temperatures at every pixel of every image. It is important to remember that the $T(t)$ resulting from these calibrations

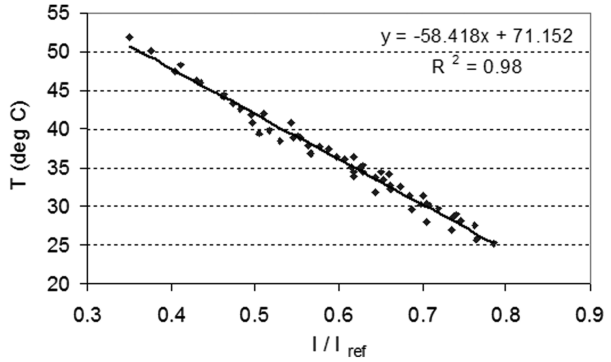

Fig. 4 Calibration curve for run 3 relating ratioed surface emission intensity to temperature under the paint layer.

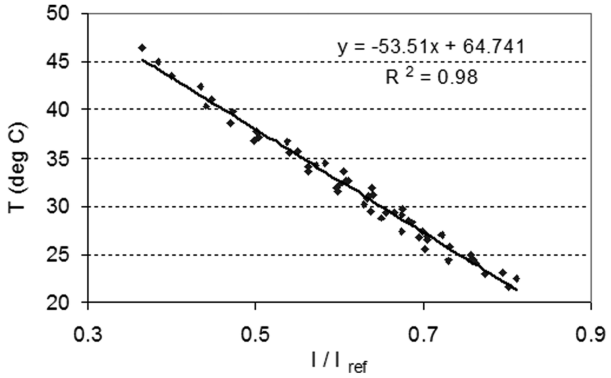

Fig. 5 Calibration curve for run 5 relating ratioed surface emission intensity to temperature under the paint layer.

are not the temperatures on the surface of the test article, but rather the temperatures that would be measured by thermocouples under the paint layer if there were a thermocouple located at every pixel under the paint layer. These temperature histories were then used as the input boundary conditions into the one-layer heat transfer data reduction algorithm described earlier.

B. Qualitative and Quantitative Heat Transfer Results

The TSP surface emission intensity data collected during runs 3 and 5 were converted into temperatures using the calibrations presented in Figs. 4 and 5, respectively. These temperature histories were used as the boundary conditions to calculate the surface convective heat transfer rates as described in detail in the heat transfer data reduction section. The heat transfer results were then nondimensionalized as Stanton number and normalized by the baseline stagnation point value. The baseline heat transfer data used for TSP data normalization and validation in the present work are the data obtained from the standard discrete instrumentation (i.e., thermocouples) during a non-TSP run at the same angle of attack and freestream conditions as the TSP runs examined here. All of the spatial coordinates were normalized by the radius of the heat shield of the test article. The resulting nondimensionalized and normalized heat transfer maps are presented in this section. To validate the heat transfer maps, the heat transfer data along several vertical section cuts where thermocouples were present under the coating were compared with the heat flux calculated from the thermocouple data from a baseline run at the corresponding locations. The plots depicting the comparison are presented in this section, as well.

The heat shield geometry itself consists of a large radius of curvature spherical portion, which transitions to a small radius of curvature toroidal part at the edges (i.e., shoulder), as illustrated in Fig. 6. Based on the geometry, the heat transfer was calculated in Cartesian coordinates everywhere on the spherical heat shield portion (i.e., surface with negligible curvature) and in cylindrical coordinates on the shoulder, where the curvature could not be neglected. It should be noted that the 1-D data reduction algorithm was not expected to yield accurate results in the shoulder area, where 2-D and 3-D heat conduction effects are most likely present due to the high spatial aeroheating gradients.

Figure 7 shows the normalized Stanton number map of the test article's heat shield at time $t = 0.7$ s for run 3. Some of the features in Fig. 7 may be best understood by examining Fig. 8, which shows the temperature-sensitive coating on the surface of the heat shield before run 3. Note that, during the first TSP application used for runs 1–4, three thermocouples on the model's surface were left unpainted. Just two thermocouples were left unpainted during the second coating application before run 5. Also note that the trip insert (an artifact from the non-TSP portion of the test program) was painted separately from the rest of the heat shield during the first coating application (runs 1–4). The entire heat shield was painted at once during the second coating application (run 5). The paint was touched-up before run 3 in the areas where it incurred damage as a result of small particle

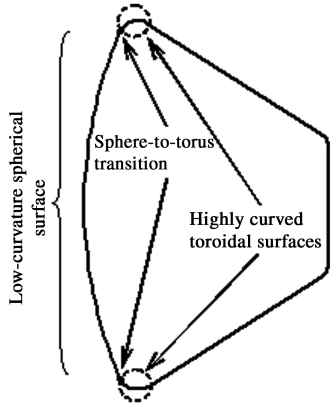

Fig. 6 Side view projection of the test article.

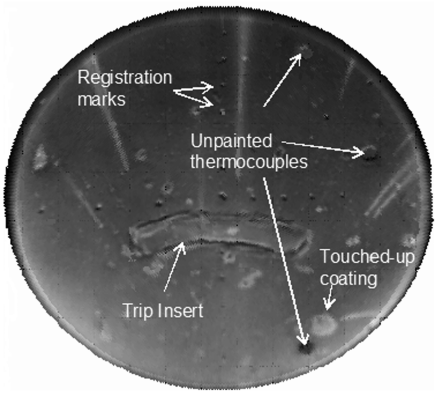

Fig. 7 Normalized Stanton number map at $t = 0.7$ s for run 3 ($M_\infty = 10$, $Re = 16.4 \times 10^6$/m).

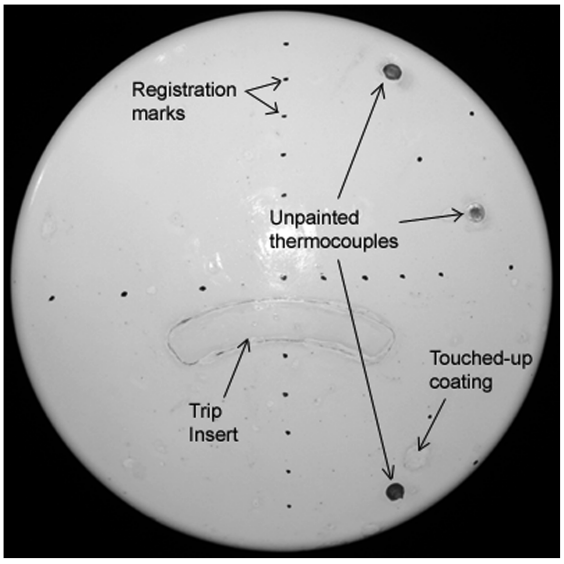

Fig. 8 Heat shield of the CEV model before run 3.

impacts during the previous high Reynolds number run (i.e., $Re = 32.8 \times 10^6$/m). The unpainted areas around the thermocouples, the trip insert, and the paint touch-ups all contributed to the unevenness of the surface of the test article during run 3. These surface defects locally affected the flow, and thus the surface heating pattern during the run, as can be seen in Fig. 7.

It is important to remember that no TSP data are available at the locations of the unpainted thermocouples, and so any apparent data in those spots are due to the image processing software extrapolating between pixels and minor image registration and mapping errors. The "streaks" appearing in the image in Fig. 7 are due to small particles impacting the test article's surface and locally disturbing the boundary layer, which results in increased localized convective heating. These features appear in all of the heat transfer maps presented in this section.

Figure 9 shows the normalized Stanton number map of the test article's heat shield at time $t = 1$ s for run 3. The normalized Stanton numbers along three section cuts where thermocouples were present under the coating are shown in Figs. 10–12, which correspond to $y/R = 0$, 0.15, and -0.4, respectively, and are marked by the three vertical dashed lines in Fig. 9. The TSP data along the section cuts are validated against the thermocouple heat-flux data obtained during a baseline run at the corresponding locations. The thermocouple heat transfer measurements at Tunnel 9 have an estimated uncertainty of $\pm 6\%$ [17]. The TSP heat transfer data appear to fall within the uncertainty margin on the majority of the heat shield surface. Some of the discrepancies between the thermocouple and the TSP data present in Figs. 10–12 are discussed next.

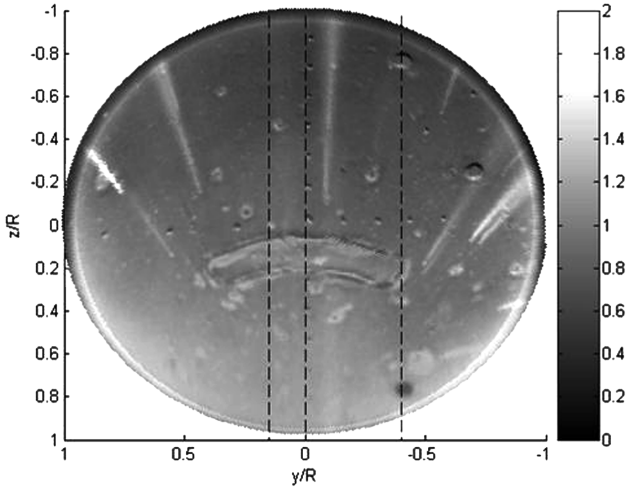

Fig. 9 Normalized Stanton number map at $t = 1$ s for run 3 ($M_\infty = 10$, $Re = 16.4 \times 10^6$/m); section cuts at $y/R = 0$, 0.15, and -0.4 are marked with vertical dashed lines.

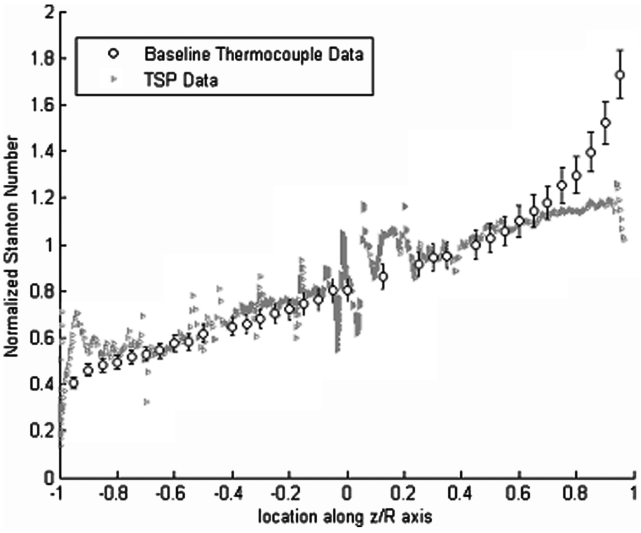

Fig. 10 Normalized Stanton number section cut at $y/R = 0$ (centerline) vs z/R location at $t = 1$ s for run 3.

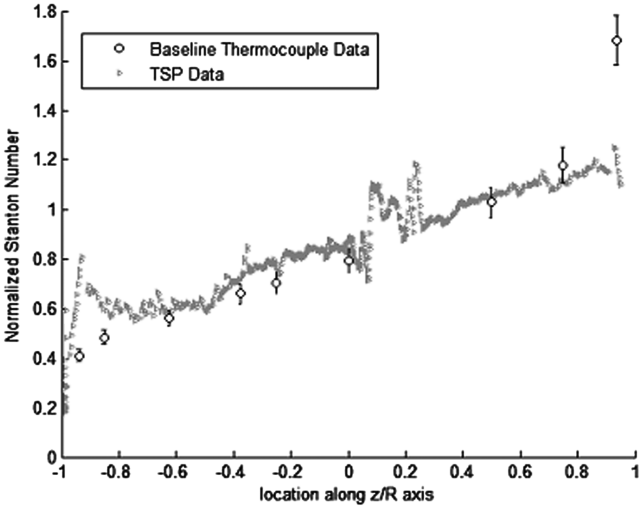

Fig. 11 Normalized Stanton number section cut at $y/R = 0.15$ vs z/R location at $t = 1$ s for run 3.

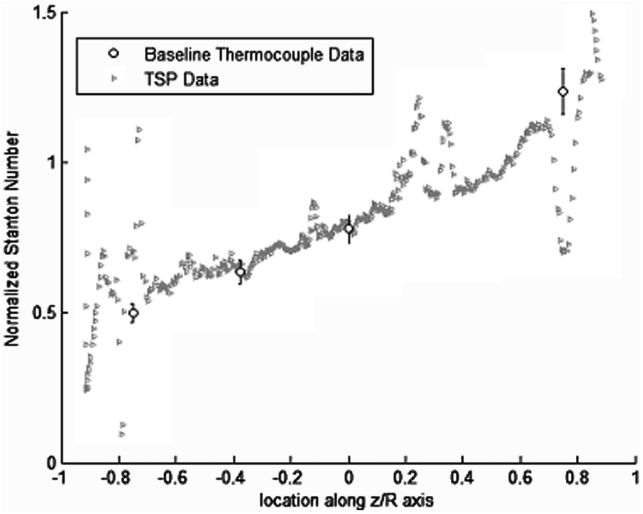

Fig. 12 Normalized Stanton number section cut at $y/R = -0.4$ vs z/R location at $t = 1$ s for run 3.

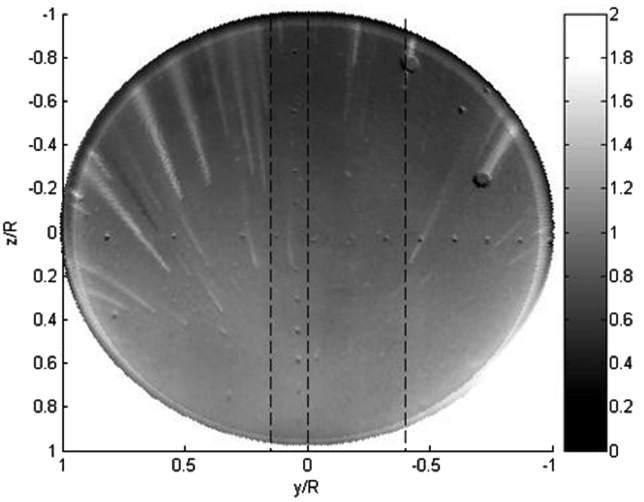

Fig. 13 Normalized Stanton number map at $t = 1$ s for run 5 ($M_\infty = 10$, $Re = 16.4 \times 10^6$/m); section cuts at $y/R = 0$, 0.15, and -0.4 are marked with vertical dashed lines.

There is a distinct spike present in the TSP data in Figs. 10 and 11 at $z/R \sim -0.94$, which in each figure corresponds exactly to the location where the heat shield geometry transitions from spherical to toroidal shape ($r/R = 0.94$), as shown in Fig. 6. The data reduction algorithm transitions from Cartesian to cylindrical coordinates at this location because the curvature of the shoulder of the heat shield is nonnegligible. The heating spike is expected to occur at this location but is absent from the thermocouple data, partly because there was no thermocouple installed at the location of the transition between the two parts of the heat shield and partly due to 2-D and 3-D heat conduction effects diffusing the sharp heating gradient. The thermocouple and the TSP data reduction algorithms are both based on a 1-D heat conduction model, so that neither technique is capable of accurately predicting convective heat transfer in the areas where multidimensional heat conduction effects are present, unless a correction is applied. However, the TSP layer acts as an insulator, so that the metal test articles coated with TSP are less prone to diffusing sharp spatial heating gradients (as compared to bare metal models) and may at least give an indication that such gradient exists. Figures 10 and 11 also point to another disadvantage of discrete instrumentation as compared to global measurement techniques: important flow features may be missed if there happen to be no sensors at the appropriate locations on a model's surface. In this case, there were no sensors on the shoulder of the model due to the difficulties associated with installing coaxial thermocouples in the highly curved region.

Each of the section cuts presented in Figs. 10–12 passes over the trip insert located in the center of the test article. Because of the unevenness and discontinuities in the coating in this area, the data in the region are scattered and should be disregarded. The TSP data between $z/R \sim -0.8$– -0.7 and $z/R \sim 0.7$–0.8 in Fig. 12 are considered invalid because the section cut on these intervals passes over the regions around two of the unpainted thermocouples, as can be seen in Fig. 9. The TSP data deviate from the thermocouple data at $z/R > \sim 0.75$ in Figs. 10 and 11. This is attributed to an extremely oblique camera viewing angle (12–24 deg) with respect to the lower quarter of the heat shield surface, which resulted in the TSP data underpredicting the heat transfer rate.

Figure 13 shows a normalized Stanton number map of the test article's heat shield at time $t = 1$ s for run 5. The heat transfer maps from runs 3 and 5 presented in Figs. 9 and 13, respectively, are very similar, that is, the heating levels and the flow patterns are similar. This is expected because the run conditions were the same for both runs. However, a few dissimilarities arise, mainly due to the differences in the quality of the coating during each of the runs. As was mentioned earlier, the coating was reapplied to the entire test article (including the trip insert) before run 5, so that the paint layer was smooth and uniform. This resulted in less flow disturbances and a smoother heating profile as compared with run 3.

Similar to run 3, no TSP data are available at the locations of the two unpainted thermocouples in the top right-hand quadrant in Fig. 13. The normalized Stanton numbers along three section cuts where thermocouples were present under the coating are shown in Figs. 14–16, which correspond to $y/R = 0$, 0.15, and -0.4, respectively, and are marked by the three vertical dashed lines in Fig. 13. Once again, the TSP data are compared with the thermocouple heat-flux data from a baseline run, which was the same run for runs 3 and 5 because the freestream conditions and the angle of attack were the same for both. The two data sets are in good agreement except for a few areas on the model's surface. The differences between the thermocouple and the TSP data present in Figs. 14–16 are discussed next.

Similar to the data from run 3, there is a distinct spike present in the TSP data in Figs. 14 and 15 at $z/R \sim -0.94$, which corresponds to the location where the heat shield geometry transitions from spherical to toroidal shape, as discussed earlier. The TSP data deviate from the thermocouple data at $z/R > 0.7$ in Fig. 14 and at $z/R > 0.8$ in Fig. 15. A similar trend was noted in the run 3 data and is attributed to an extremely oblique camera viewing angle with respect to the lower quarter of the heat shield surface. The TSP data between $z/R \sim -0.8$ and ~ -0.7 in Fig. 16 are also considered inaccurate

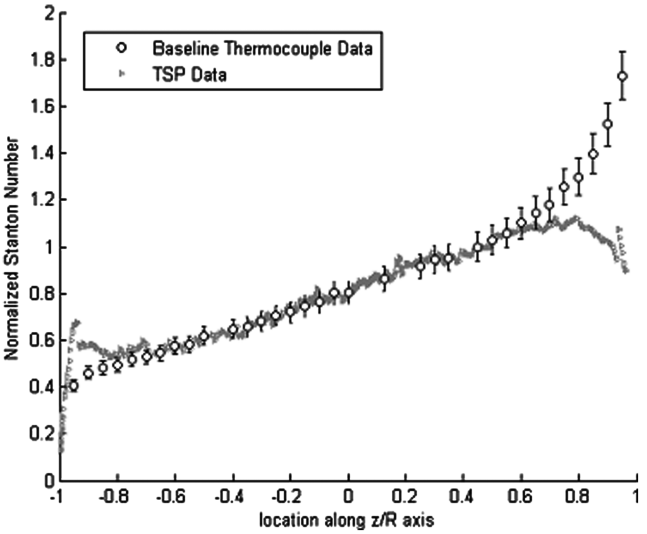

Fig. 14 Normalized Stanton number section cut at $y/R = 0$ (centerline) vs z/R location at $t = 1$ s for run 5.

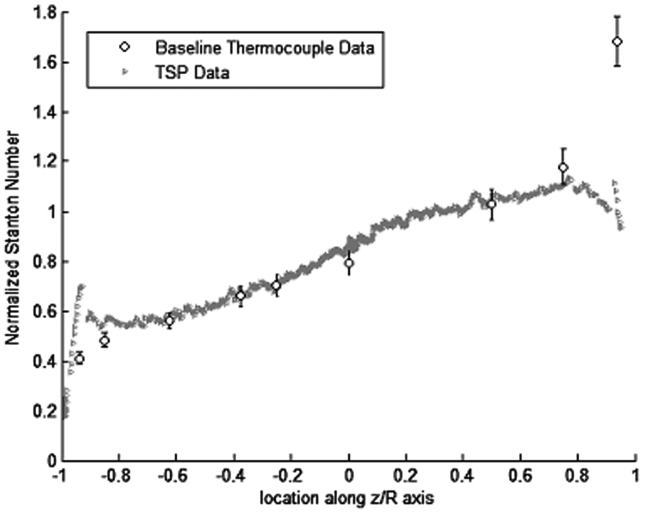

Fig. 15 Normalized Stanton number section cut at $y/R = 0.15$ vs z/R location at $t = 1$ s for run 5.

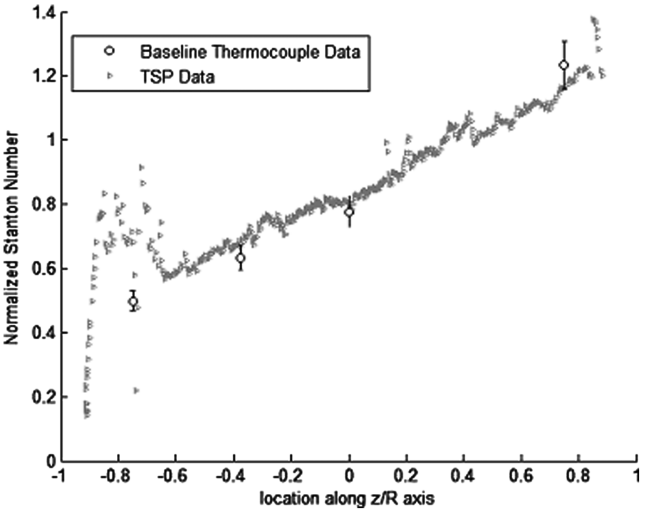

Fig. 16 Normalized Stanton number section cut at $y/R = -0.4$ vs z/R location at $t = 1$ s for run 5.

because the section cut in this interval passes over one of the unpainted regions around a thermocouple, as can be seen in Fig. 13.

A normalized Stanton number map of the heat shield for run 5 at time $t = 0.7$ s is depicted in Fig. 17. The comparison of Figs. 13 and 17 shows that the convective heating on the surface of the heat shield at 0.7 and 1 s is virtually the same. The result is expected because the Stanton number is expected to stay constant in time during the good flow portion of each run. Most of the differences in the surface heating pattern come from the hot streaks caused by small particles impacting the test article during a run, locally disturbing the boundary layer and increasing the heat flux, as was explained earlier. This phenomenon is further illustrated in Figs. 18 and 19, which show the heat transfer calculated from the TSP data and the thermocouple data from the baseline run along vertical section cuts at $y/R = 0.55$ and 0.7, respectively. The section cuts are also marked in Fig. 17 by the vertical dashed lines. The hot streaks in Fig. 17 appear as heating spikes in Figs. 18 and 19, which once again illustrates the TSP system's ability to effectively capture sharp spatial gradients and fine flow features that may be missed by discrete instrumentation. Note that the majority of the thermocouples located along the two section cuts depicted in Figs. 18 and 19 happen to coincide with the increased heating areas due to the local boundary-layer disturbances. Thus, one-to-one comparison between the baseline thermocouple and the TSP data is not possible at those locations.

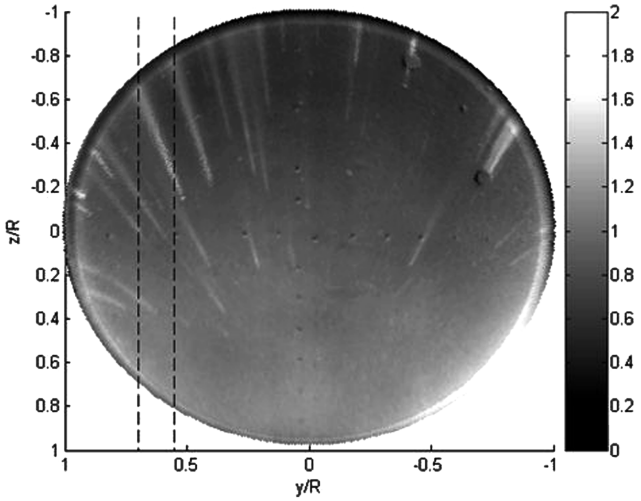

Fig. 17 Normalized Stanton number map at $t = 0.7$ s for run 5 ($M_\infty = 10$, $Re = 16.4 \times 10^6$/m); section cuts at $y/R = 0.55$ and 0.7 are marked with vertical dashed lines.

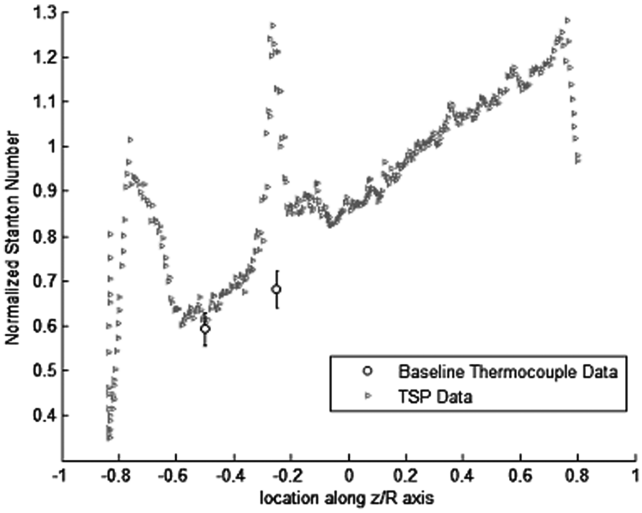

Fig. 18 Normalized Stanton number section cut at $y/R = 0.55$ vs z/R location at $t = 0.7$ s for run 5.

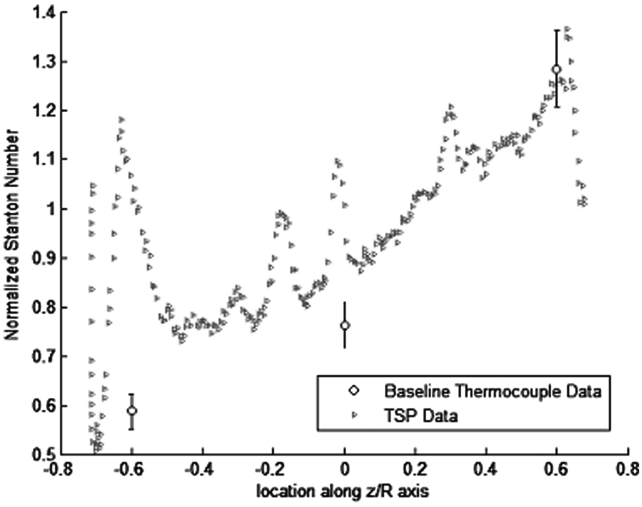

Fig. 19 Normalized Stanton number section cut at $y/R = 0.7$ vs z/R location at $t = 0.7$ s for run 5.

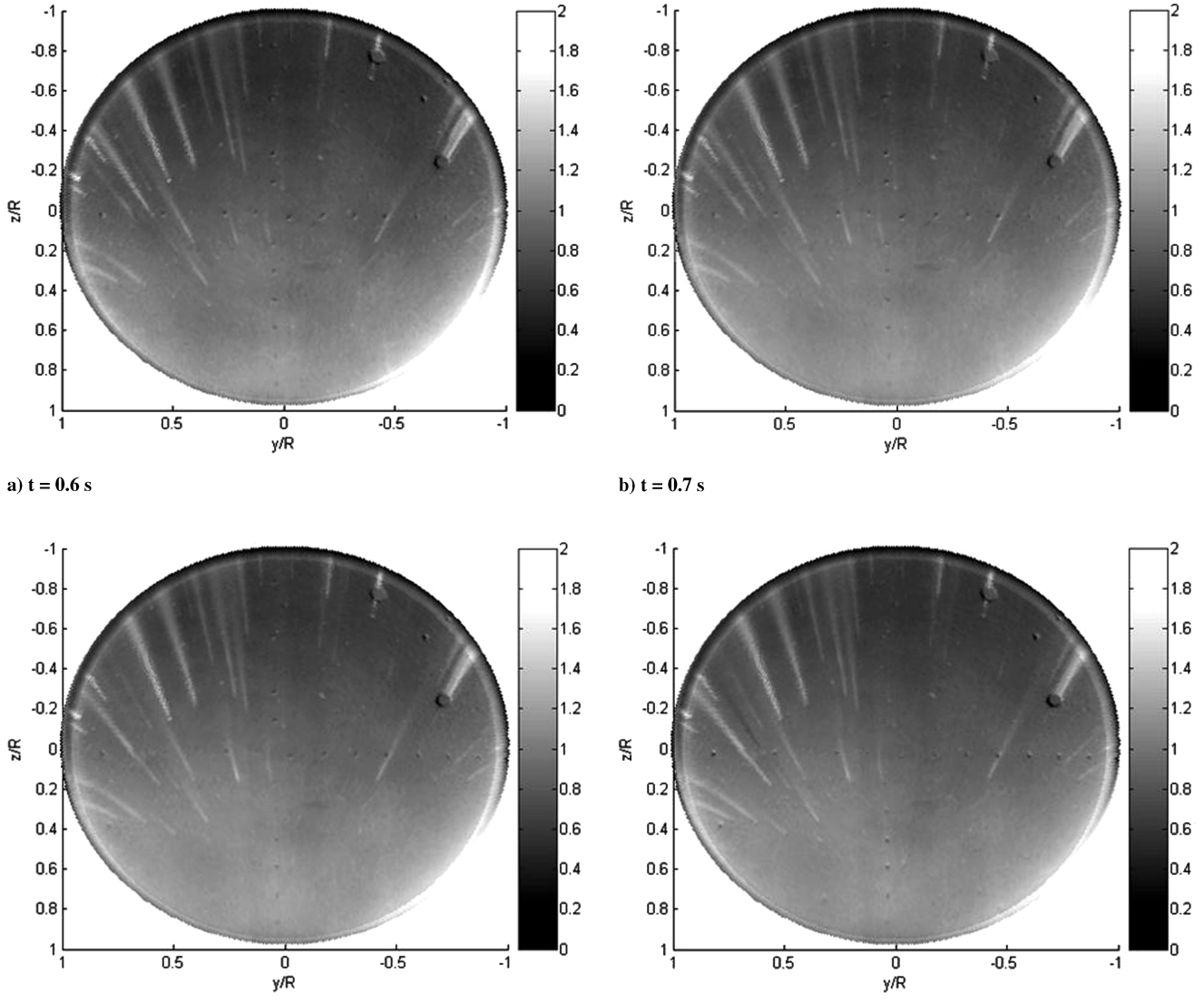

Fig. 20 Normalized Stanton number map sequence for run 5 ($M_\infty = 10$, $Re = 16.4 \times 10^6$/m).

The thermocouples that are not located in the areas of increased heating, however, track well with the TSP data.

The data reduction methodology employed here allows for the generation of heat transfer maps such as the ones in Figs. 7, 9, 13, and 17 at any instant in time during each run. A sample heat transfer map sequence obtained during the good flow period of run 5 is shown in Fig. 20, where the four images correspond to the normalized Stanton number maps at $t = 0.6$, 0.7, 0.8, and 0.9 s. Note that each image in the figure (and all other images presented earlier) is a heat transfer map at an instant in time, that is, it is not an average of several images. All four images appear to be almost identical. This is an expected result because the Stanton number is expected to stay constant during the good flow period of each static run, as was explained earlier. The ability to acquire multiple high-resolution images during each run allows for the studying of some time-varying phenomena or averaging multiple images to further improve the data quality for static runs. Quantitative heat transfer measurements during pitching runs are also possible provided a sufficiently high camera frame rate is achieved.

VIII. Conclusions

A global quantitative intensity-based TSP heat transfer measurement system was developed for the use in long-duration hypersonic facilities such as AEDC Hypervelocity Wind Tunnel No. 9. A methodology for reducing the TSP emission intensity data into convective heat flux was developed based on the current 1-D numerical scheme used for reducing coaxial thermocouple data at Tunnel 9. The proposed data reduction technique takes into consideration the ramplike heating profiles characteristic of blow-down facilities such as Tunnel 9 and can be used with metal test articles in long-duration (on the order of seconds) flows. The quantitative heat transfer measurements are currently limited to areas where there are no significant multidimensional heat conduction effects due to the 1-D nature of the algorithm. However, the system is able to resolve sharp spatial heating gradients, at least qualitatively.

The TSP system was used to collect the emission intensity data on a model of a NASA Orion CEV capsule during a five-run test program at $M_\infty = 10$, $Re = 5 \times 10^6$/ft ($\sim 16.4 \times 10^6$/m) and $Re = 10 \times 10^6$/ft ($\sim 32.8 \times 10^6$/m) conditions. The data reduction methodology was applied to the TSP data from two of the runs at $M_\infty = 10$, $Re = 5 \times 10^6$/ft ($\sim 16.4 \times 10^6$/m) condition to obtain a number of high-resolution quantitative heat transfer maps of the entire surface of the test article's heat shield. The resulting heat transfer maps were compared with the heat flux calculated from the thermocouple data collected during a non-TSP run at the same conditions. The evaluation revealed a good agreement between the two data sets. The TSP data appeared to fall within the $\pm 6\%$ thermocouple heat transfer measurement uncertainty over the majority of the model's surface for both of the runs, thus

demonstrating the ability of the TSP system to provide high-resolution global quantitative convective heat transfer measurements on metal wind-tunnel models in long-duration hypersonic flows.

Acknowledgments

The authors would like to acknowledge the financial support of NASA and the support and dedication of the Arnold Engineering Development Center Tunnel 9 team to the project. Special thanks to Marvine Hamner of LeaTech, LLC and Joseph Norris, Joe Coblish, John Lafferty, and Dan Marren of Arnold Engineering Development Center Tunnel 9 for their contributions to the work presented in the paper.

References

[1] Diller, T. E., "Time-Resolved Heat Transfer Measurements in Unsteady Flow," *1st ASME, SIAM, and APS National Fluid Dynamics Congress*, AIAA Paper 1988-3599, 1988.

[2] Kidd, C. T., and Adams, J. C., Jr., "Fast-Response Heat-Flux Sensor for Measurement Commonality in Hypersonic Wind Tunnels," *Journal of Spacecraft and Rockets*, Vol. 38, No. 5, Sept.–Oct. 2001, pp. 719–729. doi:10.2514/2.3738; also AIAA Paper 2000-2514, June 2000.

[3] Norris, J., Hamner, M., Lafferty, J., Smith, N., and Lewis, M., "Adapting Temperature-Sensitive Paint Technology for Use in AEDC Hypervelocity Wind Tunnel 9," *24th AIAA Aerodynamic Measurement Technology and Ground Testing Conference*, AIAA Paper 2004-2191, 2004.

[4] Kurits, I., Lewis, M., Hamner, M., and Norris, J., "Development of a Global Heat Transfer Measurement System at AEDC Hypervelocity Wind Tunnel 9," *22nd International Congress on Instrumentation in Aerospace Simulation Facilities*, Inst. of Electrical and Electronics Engineers, New York, June 2007, pp. 1–16. doi:10.1109/ICIASF.2007.4380905

[5] Liu, T., and Sullivan, J. P., *Pressure and Temperature Sensitive Paints*, Springer, New York, 2005, Chap. 1.

[6] Rabek, J. F., *Mechanisms of Photophysical Processes and Photochemical Reactions in Polymers*, Wiley, New York, 1987, Chap. 1.

[7] Hamner, M. P., "Demystifying Luminescent Paint Technology. A Guide for Non-Developers," *31st AIAA Fluid Dynamics Conference & Exhibit*, AIAA Paper 2001-2981, 2001.

[8] Buck, G., "Surface Temperature/Heat Transfer Measurement Using a Quantitative Phosphor Thermography System," *29th Aerospace Science Meeting*, AIAA Paper 91-0064, 1991.

[9] Merski, N. R., "Global Aeroheating Wind-Tunnel Measurements Using Improved Two-Color Phosphor Thermography Method," *Journal of Spacecraft and Rockets*, Vol. 36, No. 2, March–April 1999, pp. 160–170. doi:10.2514/2.3446

[10] Roberts, G. T., and East, R. A., "Liquid Crystal Thermography for Heat Transfer Measurement in Hypersonic Flows: A Review," *Journal of Spacecraft and Rockets*, Vol. 33, No. 6, Nov.–Dec. 1996, pp. 761–768. doi:10.2514/3.26835

[11] Nakakita, K., Osafune, T., and Asai, K., "Global Heat Transfer Measurement in Hypersonic Shock Tunnel Using Temperature Sensitive Paint," *41st Aerospace Sciences Meeting & Exhibit*, AIAA Paper 2003-743, 2003.

[12] Nagai, H., Ohmi, S., Asai, K., and Nakakita, K., "Effect of Temperature-Sensitive-Paint Thickness on Global Heat Transfer Measurement in Hypersonic Flow," *Journal of Thermophysics and Heat Transfer*, Vol. 22, No. 3, July–Sept. 2008, pp. 373–381. doi:10.2514/1.34152; also AIAA Paper 2006-1048, 2006. doi:10.2514/1.34152

[13] Hubner, J., Carroll, B., and Schanze, K., "Heat Transfer Measurements in Hypersonic Flow Using Luminescent Coating Techniques," *40th AIAA Aerospace Sciences Meeting & Exhibit*, AIAA Paper 2002-0741, 2002.

[14] Liu, T., Campbell, B. T., Sullivan, J. P., Lafferty, J., and Yanta, W., "Heat Transfer Measurement on a Waverider at Mach 10 Using Fluorescent Paint," *Journal of Thermophysics and Heat Transfer*, Vol. 9, No. 4, Oct.–Dec. 1995, pp. 605–611. doi:10.2514/3.714; also AIAA Paper 94-2484, 1994.

[15] Ragsdale, W. C., and Boyd, C. F., *Hypervelocity Wind Tunnel 9 Facility Handbook*, 3rd ed., NAVSWC TR 91-616, Naval Surface Warfare Center, Dahlgren Div., White Oak Detachment, Silver Spring, MD, July 1993.

[16] Kurits, I., "Quantitative Global Heat-Transfer Measurements Using Temperature-Sensitive Paint on a Blunt Body in Hypersonic Flows," M.S. Thesis, Dept. of Aerospace Engineering, Univ. of Maryland, College Park, MD, 2008.

[17] Hedlund, E. R., and Kammeyer, M. E., "Aerodynamic and Aerothermal Instrumentation: Measurement Uncertainty in the NSWC Hypervelocity Wind Tunnel No. 9," *19th Advanced Measurement and Ground Testing Technology Conference*, AIAA Paper 96-2210, 1996.